www.nature.com/modpathol

ARTICLE

Real-time diagnosis and Gleason grading of prostate core needle biopsies using nonlinear microscopy

Lucas C. Cahill[1,2], Seymour Rosen[3], Tadayuki Yoshitake[2], Yubo Wu[3], Linda York[4], Leo L. Tsai[4], Boris Gershman[5], James G. Fujimoto[2,6] and Yue Sun[3,6]✉

Rapid histologic assessment of fresh prostate biopsies may reduce patient anxiety, aid in biopsy sampling, and enable specimen triaging for molecular/genomic analyses and research that could benefit from fresh tissue analysis. Nonlinear microscopy (NLM) is a fluorescence microscopy technique that can produce high-resolution images of freshly excised tissue resembling formalin-fixed paraffin-embedded (FFPE) H&E. NLM enables evaluation of tissue up to ~100 µm below the surface, analogous to serial sectioning, but without requiring microtome sectioning. One hundred and seventy biopsies were collected from 63 patients who underwent in-bore MRI or MRI/ultrasound fusion biopsy procedures. Biopsies were stained in acridine orange and sulforhodamine 101, a nuclear and cytoplasmic/stromal fluorescent dye, for 45 s. Genitourinary pathologists evaluated the biopsies using NLM by translating the biopsies in real time to areas of interest and NLM images were recorded. After NLM evaluation, the biopsies were processed for standard FFPE H&E and similarities and differences between NLM and FFPE H&E were investigated. Accuracies of NLM diagnoses and Gleason scores were calculated using FFPE histology as the gold standard. Pathologists achieved a 92.4% sensitivity (85.0–96.9%, 95% confidence intervals) and 100.0% specificity (94.3–100.0%) for detecting carcinoma compared to FFPE histology. The agreement between the Grade Group determined by NLM versus FFPE histology had an unweighted Cohen's Kappa of 0.588. The average NLM evaluation time was 2.10 min per biopsy (3.08 min for the first 20 patients, decreasing to 1.54 min in subsequent patients). Further studies with larger patient populations, larger number of pathologists, and multiple institutions are warranted. NLM is a promising method for future rapid evaluation of prostate needle core biopsies.

Modern Pathology (2022) 35:539–548; https://doi.org/10.1038/s41379-021-00960-1

INTRODUCTION

Over 1 million prostate biopsy procedures are performed annually in the US[1]. Prostate biopsies are evaluated using formalin-fixed paraffin-embedded (FFPE) histology, which requires specimen processing that can take hours. Patients and urologists could benefit from a faster diagnosis, which could reduce anxiety and may reduce the number of biopsies that a clinician performs[2–6]. Rapid analysis of biopsies could also aid in triaging fresh tissue specimens for molecular/genomic analyses and research that may benefit from fresh tissue analysis. It has been reported that the lack of information about biopsies a priori can lead to suboptimal tissue allocation[7]. For example, inadequate biological specimens due to, among other things, inadequate size and cellular composition, has been identified as one of the most significant challenges in developing and validating biomarkers from tumor banks[8]. Faster biopsy analyses may also aid other investigational treatments of prostate cancer, such as focal treatment of localized prostate cancer[9].

Frozen sections are not used for rapid diagnosis of prostate biopsies because they are time- and labor-intensive, consume the small amount of tissue available, and the freezing and microtome sectioning introduce artifacts, distorting the histology and complicating interpretation[10]. Imprint cytology can be used on fresh tissue and is much faster than frozen sections, however, only a small fraction of cells are analyzed in limited contexts and the preparation process can distort the tissue and alter cellularity[11–13]. Techniques that image fresh biopsy specimens without requiring fixation, freezing, microtome sectioning, or distorting tissue could reduce the time required for biopsy analysis while preserving biopsy integrity.

Nonlinear microscopy (NLM) is a fluorescence microscopy technique that can produce high-resolution images of freshly excised tissue that resemble H&E histology. NLM scans a focused short-pulsed laser beam over a specimen to excite fluorescence only at the laser focus, generating images without microtome sectioning[14]. NLM enables imaging up to ~100 µm below the tissue surface, providing three-dimensional visualization of the tissue analogous to serial sectioning[15,16]. NLM does not affect subsequent FFPE histology analysis or immunohistochemistry assays[17]. All NLM images are digital and can easily and rapidly be

[1]Harvard-MIT Division of Health Sciences and Technology, Harvard Medical School and Massachusetts Institute of Technology, Cambridge, MA, USA. [2]Department of Electrical Engineering and Computer Science and Research Laboratory of Electronics, Massachusetts Institute of Technology, Cambridge, MA, USA. [3]Department of Pathology, Beth Israel Deaconess Medical Center, Harvard Medical School, Boston, MA, USA. [4]Department of Radiology, Beth Israel Deaconess Medical Center, Harvard Medical School, Boston, MA, USA. [5]Division of Urologic Surgery, Beth Israel Deaconess Medical Center, Harvard Medical School, Boston, MA, USA. [6]These authors contributed equally: James G. Fujimoto, Yue Sun ✉email: ysun@bidmc.harvard.edu

Received: 7 July 2021 Revised: 12 October 2021 Accepted: 13 October 2021
Published online: 2 November 2021

sent to pathologists for remote review, reducing the time required for telepathology consultation. In a previous three-pathologist blinded reading study of 122 prostatectomy specimens from 40 patients, NLM achieved a 97.3% sensitivity and 100.0% specificity for detecting prostate cancer compared to FFPE histology[18].

In this manuscript, we describe a method for evaluating prostate core needle biopsies in minutes using NLM and evaluate this method in a real-time reading of specimens from patients who underwent MRI-guided core needle biopsy procedures. The aim of this study was to assess the accuracy and procedure time of NLM for diagnosing prostate carcinoma, Gleason scoring, and estimating the amount of biopsy core involved by carcinoma.

MATERIALS AND METHODS

A total of 170 biopsies were collected from 63 patients who underwent in-bore MRI or MRI/ultrasound fusion biopsy procedures. Only targeted cores, using 18-gauge core biopsy devices, were included in this study. Written informed consent was obtained from all subjects. All research was performed according to protocols approved by Beth Israel Deaconess Medical Center Committee on Clinical Investigations and Massachusetts Institute of Technology Committee on the Use of Humans as Experimental Subjects.

Biopsy preparation

Biopsies were placed in formalin after the biopsy procedure following standard practice. The first 22 biopsies were collected for NLM imaging immediately after the biopsy procedure. Subsequent biopsies were collected for NLM imaging up to 1–3 h after the biopsy procedure to comply with COVID-19 physical distancing restrictions. The additional delay did not alter NLM images.

All biopsies from a single patient were stained in parallel with acridine orange (40 µg/ml; #10050, Electron Microscopy Sciences, Hatfield, PA) and sulforhodamine 101 (40 µg/ml; S7635, Sigma-Aldrich, St. Louis, MO) in a 1:1 ethanol:water solution for 45 s and rinsed for 1–2 s in saline. Acridine orange provided nuclear contrast and sulforhodamine 101 provided cytoplasmic/stromal contrast. The biopsies were then placed on a single microscope specimen holder with a glass window (170 µm glass thickness). Biopsy foam (30.2 ×24.5 ×2 mm (M476), Simport Scientific, Beloeil, Quebec, Canada) was used to apply gentle compression to ensure a flat imaging surface against the glass. The specimen holder was transferred to the NLM instrument.

Biopsy evaluation

The NLM instrument design was previously described[19]. A line-scan camera integrated into the NLM instrument acquired a white-light photograph of the biopsy surfaces. The white-light photograph was displayed on the computer monitor along with the NLM images and a marker indicating the position of NLM imaging that was updated in real time to aid in NLM navigation. A genitourinary pathologist evaluated the biopsies in real time by translating the specimens to areas of interest. The NLM instrument used a short-pulsed Ti:Sapphire laser (Chameleon Ultra, Coherent, Inc., Santa Clara, CA) operated at a wavelength of 1030 nm to excite acridine orange and sulforhodamine 101 fluorescence. A 20×, 0.75 NA air objective (CFI Plan Apo Lambda 20×, Nikon, Melville, NY) was used. The NLM images were updated at video rate and displayed in an H&E color scale[20]. Vertical translation of the specimen enabled evaluation of biopsies up to ~100 µm below the biopsy surface analogous to serial sectioning without the microtome. NLM images were recorded for post-procedural analysis. After NLM evaluation, the biopsies were processed for FFPE histology per standard practice.

The 15 biopsies from the first 10 patients were used to optimize tissue preparation and imaging. Previous studies interpreting cancer on multi-centimeter prostatectomy specimens served as a foundation for this optimization[17,18]. The pathologists reviewed these biopsies with NLM in real time. Then the pathologists evaluated the FFPE histology 1–2 days after the NLM evaluation. After submitting the biopsy report for clinical care, the NLM and FFPE histology were compared. This initial optimization phase improved understanding of NLM diagnoses and Gleason scoring.

The biopsies from the remaining 53 patients (155 biopsies) were read in real time with NLM by one of the pathologists who assigned a diagnosis of benign or cancer, including Gleason score and percentage of core involved by carcinoma for each core that contained cancer. Either the same pathologist or a different pathologist evaluated the FFPE histology while blinded to the NLM images.

Analysis of accuracy of detecting carcinoma and Gleason scoring

Sensitivities, specificities, positive predictive values (PPV), and negative predictive values (NPV) and 95% confidence intervals were calculated using FFPE histology as the gold standard. Cohen's Kappa was calculated between the Grade Groups assigned by NLM and FFPE histology. The correlation between the percent of core involved by carcinoma determined by NLM and FFPE histology was calculated.

RESULTS

Benign prostate biopsies

NLM images of benign prostate biopsies and corresponding FFPE H&E are shown in Fig. 1. Glandular hyperplasia is shown in Fig. 1A. The biopsy surface (left) appears hypercellular and is difficult to interpret. By translating the NLM imaging plane in the z axis (depth) in real time, tissue below the biopsy surface was evaluated. At 10 µm below the biopsy surface (center), the benign glands were more easily interpretable. Glands lined with secretory cells with abundant cytoplasm and uniform, basally positioned nuclei are clearly visualized. The corresponding FFPE H&E histology (right) shows similar benign hyperplasia. Figure 1B shows benign glands with basal and secretory cell layers visible in the NLM and FFPE H&E section. Figure 1C shows benign stroma and glands with a large corpora amylacea. The laminated structure of the corpora amylacea is seen in both the NLM image and FFPE H&E section. Glands with atrophy/post atrophic basal cell hyperplasia are seen in Fig. 1D and E on NLM images and corresponding FFPE H&E. Glandular secretory cells are visualized on NLM and FFPE H&E in the upper portion of Fig. 1E.

An NLM image and corresponding FFPE H&E section of a biopsy with seminal vesicle mucosa is shown in Fig. 2A. Closely packed glands characteristic of seminal vesicle mucosa are seen in the NLM image. The cytoplasmic yellow-brown pigment seen in seminal vesicle epithelium on FFPE H&E is not present in NLM images. Instead, unstained areas occur (arrowhead). In Fig. 2B, an NLM image of a nerve with adjacent ganglion cells (arrowheads) is seen. Nissl substance is characteristically basophilic in the NLM image.

Carcinoma

Nonlinear microscopy enabled visualization of carcinoma and recognition of Gleason patterns in prostate needle core biopsies.

Gleason pattern 3. NLM images and corresponding FFPE H&E sections of prostate needle core biopsies with Gleason pattern 3 adenocarcinoma are shown in Fig. 3. Discrete, well-formed malignant glands are clearly visualized with NLM. Bright eosinophilic secretions, as seen in Fig. 3A, C–E, are more prevalent in lumens of Gleason pattern 3 adenocarcinoma glands in tissues visualized with NLM than on FFPE H&E sections. These secretions can appear solid, as in Fig. 3A, D, E or have a crystalline appearance as in Fig. 3C. Pattern 3 glands can also appear without eosinophilic secretions as shown in Fig. 3B.

Foamy gland carcinoma does not have the characteristic foamy appearance usually seen on FFPE H&E in NLM images (Fig. 3C). Foamy gland carcinoma visualized using NLM has the same architectural features as FFPE H&E section, namely discrete, well-formed glands that are often closely packed. Many cytological features are also similar to FFPE H&E sections, such as smaller, basally located nuclei without prominent nucleoli with abundant cytoplasm, but the cytoplasm appears eosinophilic and denser on NLM than on FFPE H&E sections. These similar architectural and cytologic features enable identification of foamy gland carcinoma.

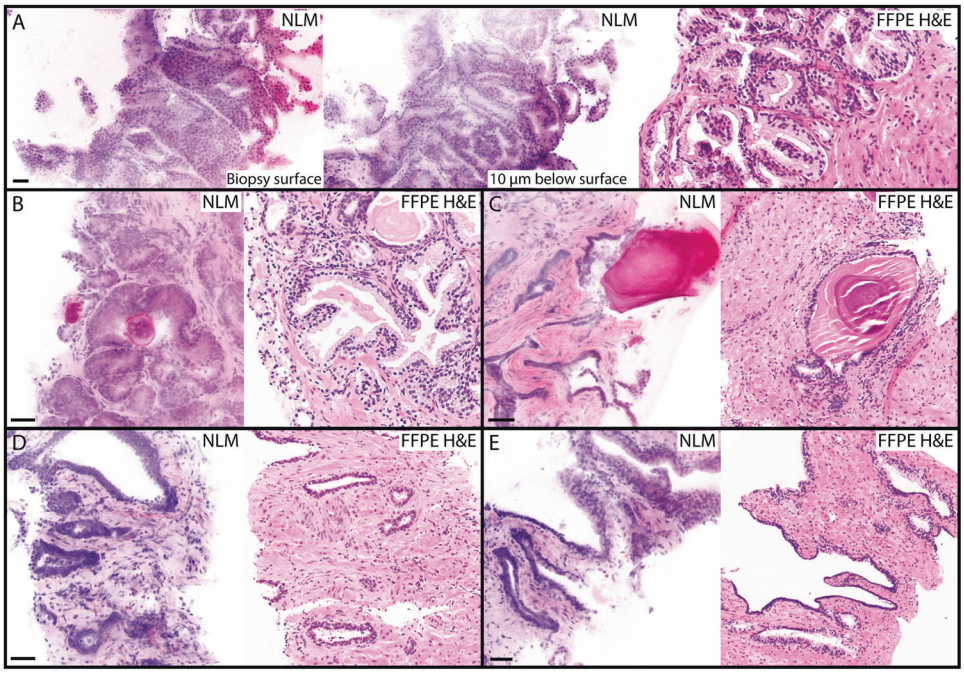

Fig. 1 Nonlinear microscopy (NLM) images of benign prostate needle core biopsies. A An NLM image of glandular hyperplasia acquired at the biopsy surface (left), at 10 µm below the biopsy surface (center), and a corresponding formalin-fixed paraffin-embedded (FFPE) H&E section (right). The surface of biopsies can often appear hypercellular and can be difficult to interpret. **B** Benign glands with a basal and secretory cell layers visualized in an NLM image (left) and a corresponding FFPE H&E section (right). **C** Benign glands with a large corpora amylacea (NLM: left, FFPE H&E: right). **D** Atrophy/post atrophic basal cell hyperplasia (NLM: left, FFPE H&E: right). **E** Atrophy/post atrophic basal cell hyperplasia (bottom) with a glandular secretory cell component (top) (NLM: left, FFPE H&E: right). Scale bars = 50 µm.

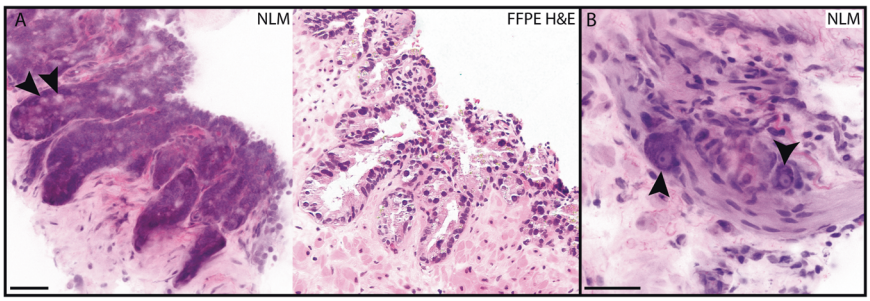

Fig. 2 Nonlinear microscopy (NLM) images of seminal vesicles and nerves from prostate needle core biopsies. A An NLM image (left) and a corresponding formalin-fixed paraffin-embedded (FFPE) H&E section (right) of seminal vesicle mucosa. Yellow-brown pigment in the cytoplasm does not stain in NLM (arrowhead). **B** An NLM image of a nerve with adjacent ganglion cells. The prominent nucleoli of ganglion cells (arrowhead) are apparent. Nissl substance stains basophilic on NLM. Scale bars = 50 µm.

Gleason pattern 3 glands can appear solid as shown in Fig. 3D. In this case, gland lumens are difficult to visualize on NLM. However, the densely-packed glandular architecture and eosinophilic intraluminal secretions make the diagnosis of cancer apparent. Perineural invasion is also readily identifiable on NLM as shown in Fig. 3E.

NLM images and corresponding FFPE H&E of Gleason pattern 3 with small discrete glands are shown in Fig. 4. Interpretation of such areas can be problematic and can appear to be merging into pattern 4. Carcinoma infiltrating the prostatic stroma between benign glands is shown in Fig. 4B. The benign glands are easily identifiable on the NLM image and the basal and secretory cell layers are seen.

Gleason pattern 4. NLM images and corresponding FFPE H&E sections of prostate needle core biopsies with Gleason pattern 4 adenocarcinoma are shown in Fig. 5 and Supplementary Fig. 1. Fused glands in a cribriform pattern, characteristic of Gleason pattern 4, are readily visualized in NLM images. Gleason pattern 4 admixed with pattern 3 is shown in Fig. 5C, D, F and Supplementary Figure 1. In C, the pattern 3 glands are small whereas in F, the pattern 3 glands are large and have eosinophilic intraluminal secretions. Similar to FFPE H&E sections, NLM images of Gleason pattern 4 rarely contain intraluminal secretions. Gleason pattern 4 with glandular lumens occluded by proliferating cells is shown in Fig. 5D. Clear cytoplasmic vacuoles are visualized on NLM images and FFPE H&E sections (inset). A glomeruloid pattern is shown in Fig. 5D–F. The cribriform proliferation attached to one edge of the gland giving the characteristic glomeruloid appearance is apparent in both the NLM image and FFPE H&E.

Mucin-producing prostatic adenocarcinoma from prostate needle core biopsies is visualized in NLM images and corresponding FFPE H&E in Fig. 6 and Supplementary Fig. 2. Rapid evaluation of tissue below the biopsy surface with NLM enabled analysis of the cribriform pattern in this biopsy at multiple depths (Fig. 6B). The blue tinge seen in mucin on FFPE H&E sections is not present on NLM images of fresh prostate biopsies. This could be partly due to the different staining characteristics of hematoxylin versus

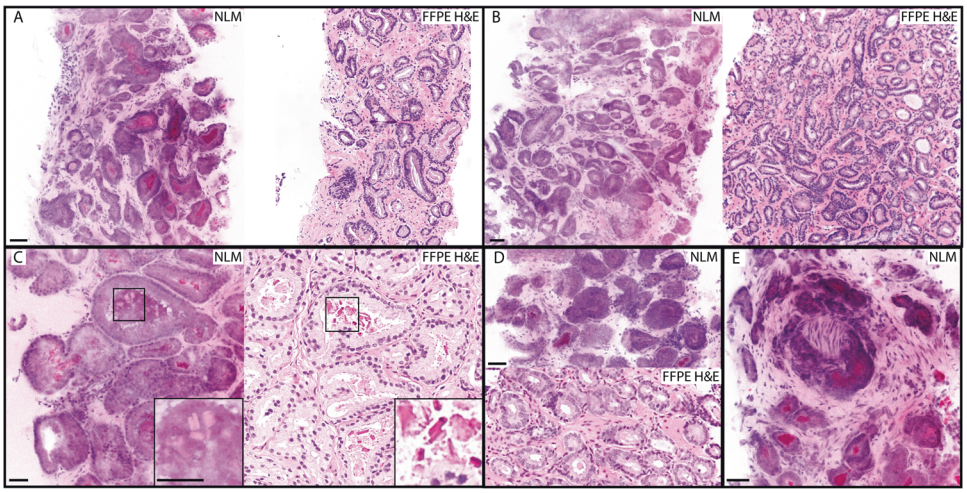

Fig. 3 Nonlinear microscopy (NLM) images of Gleason pattern 3 prostatic adenocarcinoma from prostate needle core biopsies. A Discrete, well-formed glands are clearly visualized with NLM (left) and formalin-fixed paraffin-embedded (FFPE) H&E (right). Bright, solid eosinophilic secretions are more commonly seen in these NLM images of Gleason pattern 3. **B** Gleason pattern 3 without eosinophilic secretions (NLM: left, FFPE H&E: right). **C** An example of foamy gland adenocarcinoma (NLM: left, FFPE H&E: right). The cytoplasm of secretory cells visualized using NLM does not have the characteristic foamy appearance present in FFPE H&E. The intraluminal secretions may have a crystalline appearance (inset). **D** Malignant glands that appear solid (NLM: top, FFPE H&E: bottom). **E** An example of an NLM image showing perineural invasion (center). Scale bars = 50 µm.

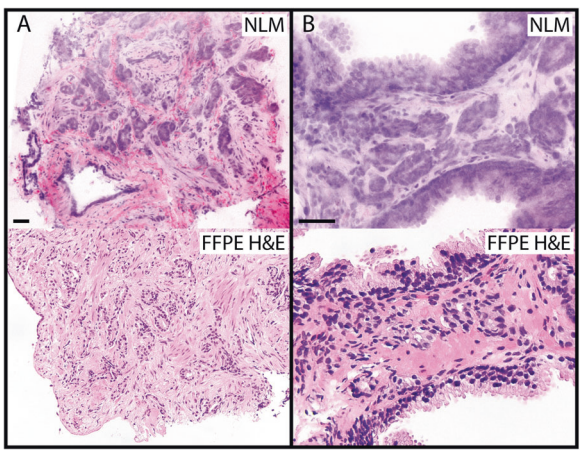

Fig. 4 Nonlinear microscopy (NLM) images of Gleason pattern 3 prostatic adenocarcinoma with small glands in prostate needle core biopsies. Interpretation of such areas can be problematic and can appear to be merging into pattern 4. **A** Small discrete glands (NLM: top, formalin-fixed paraffin-embedded (FFPE) H&E: bottom). **B** Malignant glands infiltrating the prostatic stroma between benign glands (NLM: top, formalin-fixed paraffin-embedded (FFPE) H&E: bottom). Basal and secretory cell layers are seen in the benign glands in the NLM image and FFPE H&E section. Scale bars = 50 µm.

acridine orange. It is also likely due to the mucin not being fixed to the glands and therefore the mucin is free floating in fresh tissue. The free-floating mucin partially covers the surface of the biopsy core, occluding NLM imaging in some areas (light appearance in dashed oval in Fig. 6A).

Gleason pattern 5. NLM images and corresponding FFPE H&E sections of prostate needle core biopsies with Gleason pattern 5 adenocarcinoma are shown in Fig. 7. Sheets of tumor cells with prominent nucleoli lacking gland formation are seen in the NLM image and corresponding FFPE H&E section in Fig. 7A. NLM images of cords and strands of malignant cells are shown at two different depths below the biopsy surface in Fig. 7B. Multiple depths confirmed that gland lumen formation was minimal, consistent with Gleason pattern 5, which is confirmed on the corresponding FFPE H&E section (bottom). Extraprostatic extension, with carcinoma in adipose tissue, is also clearly visualized with NLM as shown in the inset of Fig. 7B, which is an image from another area of the biopsy. Friable, high-grade tumor can appear loosely connected to the prostate stroma in NLM images of fresh biopsy tissue (Fig. 7C). Since the tissue is not fixed or embedded in paraffin, the top layer of stained tumor cells can become detached from the biopsy and appear beside the main core (orange arrowhead, bottom). Migration of these tumor cells out of the core leaves an area of weakly stained cells, which have minimal NLM signal (black arrowhead).

Variation of pathology at different depths. Visualizing core biopsies at multiple different depths with NLM enables an evaluation that is more comprehensive than FFPE H&E without requiring laborious and time-consuming serial sections in areas of uncertainty. Figure 8A demonstrates NLM analysis of variation in pathology in depth. A nerve free of carcinoma is present 12 µm below the surface (dashed circle) while perineural invasion is identified at 22 µm depth (B, dashed circle). Visualizing multiple depths can augment the assessment of Gleason patterns. Figure 8C–E shows a biopsy with large, malignant glands with intraluminal secretions adjacent to chronic inflammation and benign glands. D. and E. are NLM images acquired 4 µm and 8 µm below C, respectively. In C, there appears to be a potential focus of glands in a cribriform pattern (black box) that evolves into a single discrete gland in E.

Accuracy of detecting carcinoma and Gleason scoring

Eighty-seven biopsies from 39 lesions in 36 patients were positive for carcinoma on FFPE histology. The sensitivities and specificities for detecting carcinoma on NLM on a per-biopsy basis were 92.4% and 100%, on a per-lesion basis were 92.3% and 100%, and on a per-patient basis were 91.7% and 100% (Table 1).

Seven biopsy cores were falsely diagnosed as benign on NLM. All 7 of these biopsies were Grade Group 1 on FFPE H&E. Two of these false negatives were from two patients who had less than 5% of the core involved with carcinoma on FFPE H&E. These false negatives likely resulted from a mismatch in NLM imaging plane

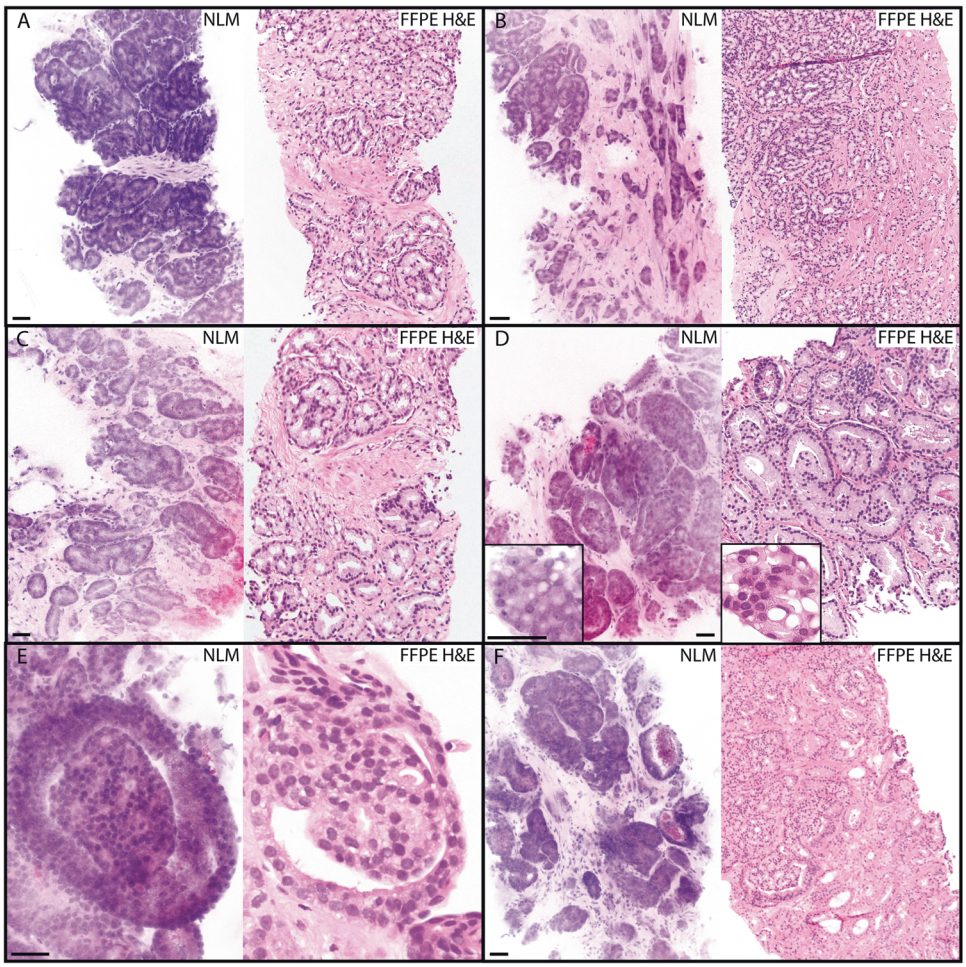

Fig. 5 Nonlinear microscopy (NLM) images of Gleason pattern 4 prostate adenocarcinoma from prostate needle core biopsies. A Typical Gleason pattern 4 with fused glands in a cribriform pattern. **B** Distinct areas of Gleason pattern 4 on the left side of the biopsy and pattern 3 on the right side of the biopsy. **C** Gleason pattern 4 with a component of pattern 3 throughout the image. **D** Gleason pattern 4 with glandular lumina occluded by proliferating cells. Cytoplasmic vacuoles are seen (inset). **E** A glomeruloid pattern. **F** Gleason pattern 4 with a cribriform structure admixed with pattern 3. The Gleason pattern 3 is composed of large distinct glands with intraluminal secretions (right). In contrast, the Gleason pattern 4 does not contain intraluminal secretions. A-F NLM: left, formalin-fixed paraffin-embedded (FFPE) H&E: right. Scale bars = 50 µm.

and FFPE H&E sectioning plane. Two false negatives were from a single patient that had a low-grade carcinoma and an appearance that had not previously been seen on NLM (small malignant glands). Low-grade carcinomas with small malignant glands were correctly diagnosed with NLM in later biopsies in this study and do not present a problem once the pathologist is well-trained to interpret these images. False negatives on 3 biopsies from 2 patients occurred on the same day after a 5-month gap in this study due to the COVID-19 clinical research stoppage, and were likely due to the lack of recent NLM experience. After these false negatives, pathologists were retrained on previous data sets. Upon review of the 5 false negatives with greater than 5% of the core involved with carcinoma, the carcinoma was apparent on NLM.

Table 2 demonstrates the concordance for Gleason Grade Groups of each prostate biopsy determined using NLM and FFPE H&E histology on a per-biopsy basis. The Gleason score could not be determined in three biopsies on NLM and two biopsies on FFPE H&E because only a small focus of carcinoma was present in the biopsy or because fragmentation of the biopsy core made interpretation challenging. The agreement between the Grade Group determined by NLM and the Grade Group determined by FFPE H&E had a Cohen's Kappa of 0.588.

The estimated percent of the core involved with carcinoma determined using NLM versus FFPE histology had a Pearson's correlation coefficient of 0.617. The mean absolute difference between the percent of core involved with carcinoma determined with NLM versus FFPE histology was 17.5%.

The time required to evaluate biopsies using NLM is shown in Table 3. The mean time to prepare biopsies for NLM evaluation was 2.45 min (standard deviation (SD) = 0.78 min), the mean NLM evaluation time per biopsy was 2.10 min (SD = 1.42 min), and the mean total time (preparation + evaluation time) per patient was 8.15 min (SD = 4.16 min). The mean evaluation time per biopsy in the first 20 patients was double the evaluation time in the remaining patients. The total time per patient has a large standard deviation since the time required to evaluate all biopsies depends on the number of biopsies evaluated, which varied from 1 to 9 (median of 3 biopsies).

DISCUSSION

NLM enables interpretation of prostate biopsies in minutes without affecting subsequent FFPE histology analysis or immunohistochemistry assays[17]. Features of benign tissue, such as benign glands with basal and secretory cell layers, benign stroma with fibroadipose tissue, nerves, and vessels, and glandular and basal cell hyperplasia were readily visualized with NLM. Features of carcinoma, such as small, infiltrating glands that lack basal cells,

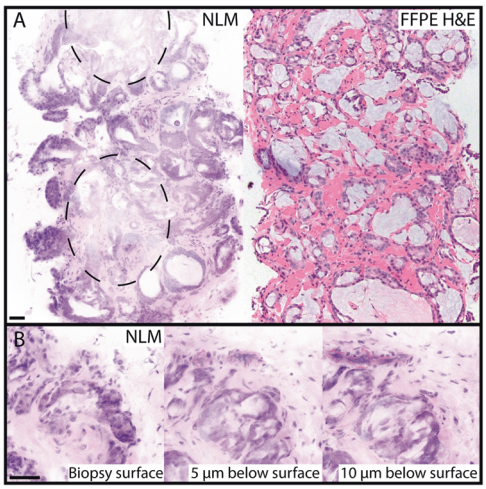

Fig. 6 Nonlinear microscopy (NLM) images of mucin-producing prostatic adenocarcinoma from prostate needle core biopsies. A An NLM image (left) and a corresponding formalin-fixed paraffin-embedded (FFPE) H&E section (right). Mucin does not stain in NLM images and therefore the blue tinge seen in the FFPE H&E is not present in NLM. In NLM evaluation of fresh tissue, the mucin covers the surface of the biopsy (dashed oval) and thus occludes NLM imaging. This occlusion appears as lighter regions (dashed circle) throughout the biopsy. **B** NLM images acquired at the surface and 5 µm and 10 µm below the surface of the biopsy shown in **A**. The cribriform pattern varies in depth. Scale bars = 50 µm.

nuclear enlargement, and prominent nucleoli, were visualized well with NLM. Furthermore, Gleason patterns could be differentiated, including the discrete, well-formed glands of Gleason pattern 3, cribriforming, fused glands, and glomeruloid patterns of Gleason pattern 4, and the sheets of cells with minimal gland formation of Gleason pattern 5.

The sensitivity and specificity of detecting carcinoma using NLM on a per-biopsy, per-lesion, and per-patient basis did not vary significantly and were ~92% and 100%, respectively. The similarities between NLM and FFPE H&E reduce training requirements for interpretation and makes NLM a promising technique for rapid prostate biopsy diagnosis. However, it is important to recognize that NLM images are not identical to FFPE H&E sections. Misunderstandings can result from relying too heavily on previous FFPE H&E experience. It is critical that the pathologist understands the differences in fresh tissue NLM imaging in order to confidently and accurately interpret images. We characterize these differences below to enable more accurate interpretation of NLM images.

Similarities/Differences

Dehydrated, paraffinized tissue versus fresh tissue. Paraffin processing, which includes formalin fixation, alcohol dehydration, and paraffin embedding, results in reduced tissue volume, cell shrinkage, and cytoplasmic retraction. As a result, when compared to paraffin processed tissue, NLM images of structures such as glands and cells visualized on fresh tissue appear thicker and more crowded (example: Fig. 1A). Furthermore, the cell borders in fresh tissue are less sharp due to this crowding and they have rounder, fuller appearing cytoplasm. NLM images also have larger and more frequent prominent nucleoli throughout carcinoma compared to FFPE H&E, which can be a useful diagnostic feature.

Visualization of tissue prior to paraffin processing also results in additional cytoplasmic and luminal contents being present. For example, in the foamy gland variant of carcinoma, the characteristic foamy cytoplasm is not present on NLM and instead eosinophilic contents are seen (Fig. 3C). Luminal contents, such as intraluminal secretions in low-grade carcinoma (Gleason 3), are more frequent in NLM than FFPE H&E likely due to the removal of these contents with FFPE processing. The frequent and clearly identifiable secretions are a useful diagnostic marker in NLM and may help differentiate benign hyperplasia.

Physical sectioning with a microtome versus optical sectioning. Unlike in FFPE histology where the axial resolution is determined by the thickness of microtome sections and lateral resolution is determined by the objective lens and microscope condenser, both the axial and lateral resolution in NLM imaging of thick tissue specimens is determined by the objective and laser beam focus. A higher NA/power objective provides finer axial resolution (equivalent to a thinner section) enabling greater differentiation of architectural (Gleason patterns) and cytological details. For example, when changing from a 5× to 10× objective, the field of view is reduced by one half in both NLM and FFPE histology. However, the thickness of tissue visualized with NLM when changing from a 5× to 10× objective ranges from ~20 µm to ~8 µm (depending on the objective NA), whereas the FFPE H&E always has a 5 µm physical thickness. This fact is important to recognize when interpreting images since when the axial section thickness increases, glands appear more crowded potentially resulting in false positive diagnoses.

There is a tradeoff between image resolution and speed in NLM evaluation. With larger prostatectomy specimens, a 10×, 0.45 NA objective enabled accurate and rapid cancer diagnoses, as described previously[18], however the limited axial (z) resolution made differentiation of Gleason patterns in biopsies difficult. In this study we used a 20×, 0.75 NA objective which improved visualization of architectural and cytological details, but had a smaller field of view. It is important to note that NLM can use multiple objectives interchangeably like a traditional histology microscope[19] and therefore is not limited to a single resolution.

White-light transillumination versus fluorescence microscopy. FFPE H&E and NLM microscopy images are generated using different physical processes. FFPE H&E evaluation is performed using transillumination microscopy with white light. In transillumination microscopy, areas of higher dye concentration absorb more light and appear darker. NLM images are generated using epi-illumination and fluorescence detection. Areas of higher dye concentration have more fluorescence emission and generate more signal. To visualize the NLM images in an H&E color scale, fluorescence signals are remapped using a technique known as Virtual Transillumination Microscopy (VTM)[20]. VTM enables colors and intensities of the nuclear and cytoplasmic/stromal channels to be individually adjusted to suit the user's preference in real time.

White-light transillumination of an FFPE H&E slide also enables the entire visible spectrum of colors to be visualized, whereas NLM uses two discrete color channels, which collect the fluorescence from the acridine orange and sulforhodamine 101. Therefore, only combinations of the two color hues that correspond to the two channels are represented in NLM. Features that rely on color are less apparent, less consistent, or impossible to generate. For example, the bright red appearance of red blood cells and the yellow-brown pigment in seminal vesicles are not visualized on NLM.

Staining with hematoxylin and eosin versus acridine orange and sulforhodamine 101. Acridine orange and sulforhodamine 101 have slightly different staining specificities than hematoxylin and eosin. For example, distinct pink elastic fibers can be seen throughout the stroma and in the elastic lamina of vessels on NLM that are not present on FFPE H&E. Mucin is not stained with acridine orange or sulforhodamine 101, leaving areas of mucin absent of NLM signal. Furthermore, staining can also be less homogenous in NLM than in FFPE H&E, likely due to the loss of viability and permeabilization of FFPE sections, resulting in variations in cytoplasmic colors between or within biopsies in NLM images.

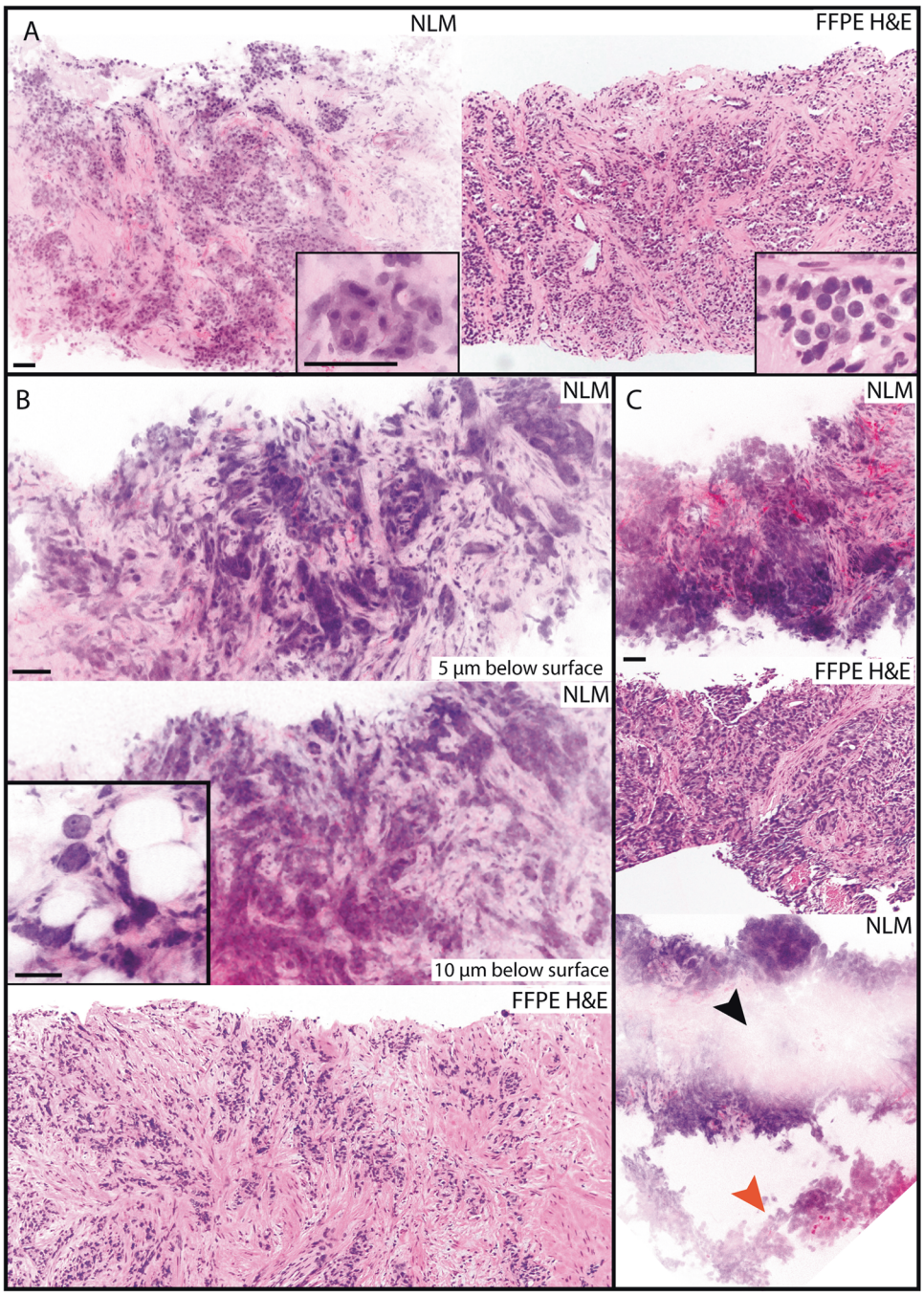

Fig. 7 Nonlinear microscopy (NLM) images of Gleason pattern 5 prostatic adenocarcinoma from prostate needle core biopsies. A Gleason pattern 5 consisting of sheets of tumor cells without gland formation (NLM: left, corresponding formalin-fixed paraffin-embedded (FFPE) H&E: right). A high magnification image (from a different depth below the surface of the same biopsy) showing prominent nucleoli is shown inset. **B** An NLM image of Gleason pattern 5 consisting of cords and strands of cells with minimal lumen formation acquired 5 µm below the biopsy surface (top), an NLM image acquired 10 µm below the biopsy surface (center), and a corresponding FFPE H&E (bottom). Evaluating NLM images at multiple depths confirmed that gland lumina were limited. The inset shows carcinoma in adipose tissue from another area of the biopsy. **C** An NLM image of a high-grade tumor that appears loosely connected to the stroma (top) and a corresponding FFPE H&E section (center). In another area of the biopsy, the top layer of stained tumor cells became detached from the biopsy (orange arrowhead) in the NLM image and migrated out of the main core specimen (bottom). The detachment of tumor cells leaves an area of weakly stained tissue, which is absent of NLM signal (black arrowhead). Scale bars = 50 µm.

Two dimensional versus three-dimensional analysis. The ability of NLM to rapidly evaluate multiple depths in tissue can be advantageous. For example, the multiple image depths in Fig. 1A are used to more clearly define benign tissue, in Fig. 6A to define the cribriform structure in mucin-producing carcinoma, and in Fig. 7A to verify that there is minimal or no glandular formation in a biopsy with Gleason pattern 5. However, imaging multiple depths can also complicate biopsy evaluation. Classification of prostate carcinoma with Gleason scores is important for predicting clinical course and disease behavior[21]. Gland formation that is distinct and individual is associated with less aggressive tumors. Conversely, architectural complexity and loss of gland formation

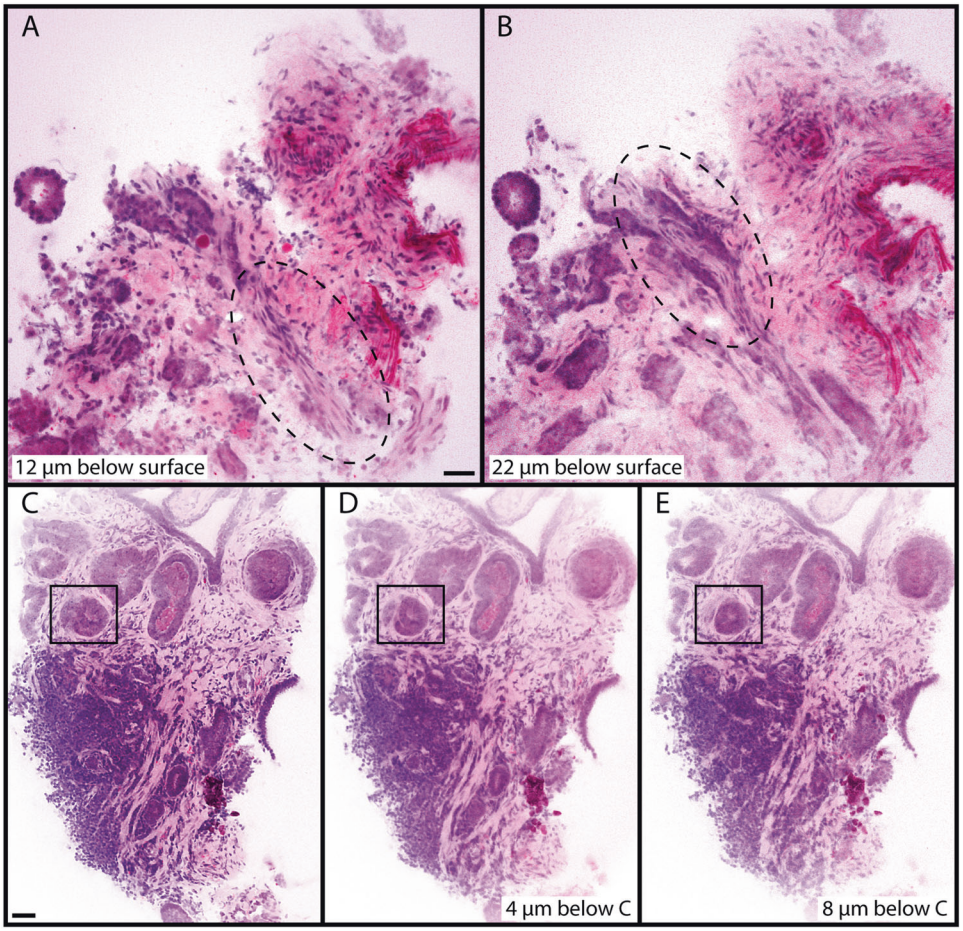

Fig. 8 Pathology variations when changing the depth (z axis) of nonlinear microscopy (NLM) imaging. A A nerve (dashed circle) uninvolved by carcinoma at 12 µm below the biopsy surface becomes (**B**) involved by carcinoma 22 µm below the tissue surface. **C** Large, malignant glands with intraluminal secretions adjacent to chronic inflammation and benign glands. **D** and **E** are NLM images acquired 4 µm and 8 µm below **C**, respectively. In **C**, there appears to be a potential focus of cribriform pattern (black box), which evolves into a single discrete gland in **E**. Scale bars = 50 µm.

Table 1. Summary of sensitivity and specificity of prostate biopsies evaluated using nonlinear microscopy (NLM).

	Biopsies (Total = 155)	Lesions (Total = 62)	Patients (Total = 53)
Sensitivity [95% CI]	0.924 [0.850,0.969]	0.923 [0.791, 0.984]	0.917 [0.775, 0.983]
Specificity [95% CI]	1.000 [0.943, 1.000]	1.000 [0.852, 1.000]	1.000 [0.805, 1.000]
PPV	1.000	1.000	1.000
NPV	0.900	0.885	0.850
Accuracy	0.955	0.952	0.943

PPV positive predictive value, *NPV* negative predictive value, *CI* confidence interval.

Table 2. Comparison of Grade Groups determined using nonlinear microscopy (NLM) and formalin-fixed, paraffin-embedded (FFPE) H&E slides.

		NLM					
	Grade Group	Benign	1	2	3	4	5
FFPE H&E	Benign	63	0	0	0	0	0
	1	7	24	6	0	0	0
	2	0	1	22	9	0	0
	3	0	0	2	7	0	0
	4	0	0	0	1	3	0
	5	0	0	1	2	1	1

portends an increased malignant potential. Several groups, however, have shown that Gleason patterns change throughout the depth of individual biopsies[22–24]. This complicates the comparison of FFPE H&E and NLM, especially in cases of clearly glandular Gleason 3 pattern vs gland fusion/luminal narrowing Gleason 4 pattern (Fig. 8). Sections at multiple depths are typically evaluated in FFPE histology, but NLM can image continuous variations in depth in real time, enabling volumetric assessment. This is a unique capability for assessing tumor characteristics that may improve upon two-dimensional visualization in FFPE.

Necrotic/high-grade areas. Biopsies that are necrotic or friable, such as in cases of high-grade carcinoma, have cells that slough off during manipulation. Since the biopsies are not stabilized and supported through fixation and paraffinization, these cells can float off the biopsy and appear in different regions of the biopsy, leaving areas devoid of stained cells (Fig. 7C).

Table 3. Evaluation time of prostate biopsies using nonlinear microscopy (NLM).

	Mean	Median	Standard deviation
Preparation time/ patient (min)	**2.45**	**2.19**	**0.78**
Patient #1–20	*2.49*	*2.50*	*0.72*
Patient #21–53	*2.43*	*2.08*	*0.82*
Evaluation time/ biopsy (min)	**2.10**	**1.68**	**1.42**
Patient #1–20	*3.08*	*2.58*	*1.81*
Patient #21–53	*1.54*	*1.36*	*0.70*
Total time/patient (min)	**8.15**	**6.89**	**4.16**
Patient #1–20	*8.85*	*8.00*	*4.75*
Patient #21–53	*7.75*	*6.83*	*3.81*

The number of biopsies evaluated for a single patient varied from 1 to 9 with a median of 3 biopsies.
The bold values are total times.
The italics values are specific times for the corresponding patients.

Blood. Large amounts of blood in the biopsy can confound interpretation. The blood prevents adequate staining of the biopsy, causing regions to have limited NLM signal and appear white (Supplementary Fig. 3). Since blood itself is also stained minimally with acridine orange or sulforhodamine 101, little signal is generated. This effect could obscure pathology (although we have not observed this in any cases we evaluated) or make determination of Gleason scores and extent of tumor difficult.

Surface artifacts. Core needle biopsies usually have obscuring artifacts, such as debris from gauze or tissues, are hypercellular (Fig. 1A), and have loose cells on their surfaces due to damage from the biopsy needle or handling the fragile tissue (Fig. 7C). These artifacts are not present on FFPE histology since slides are obtained from subsurface tissue after facing the paraffin block. The capability of visualizing subsurface tissue with NLM is critically important for interpretation of fresh biopsy tissue.

NLM accuracy and speed

Gleason scoring typically has high interobserver variability. The agreement between the Grade Group determined by NLM and by FFPE H&E was moderate and is within the average kappa values reported in the literature between general pathologists (0.41) and urologic pathologists (0.59)[25]. In addition, Gleason patterns change throughout the depth of individual biopsies[22–24]. This means that variations in NLM imaging and FFPE H&E sectioning plane can alter Gleason scores. Furthermore, NLM can image continuous variations in depth in real time, which enables volumetric assessment and can make Gleason score comparisons to a two-dimensional histological section challenging.

A major discrepancy in Grade Groups occurred in one biopsy where a Grade Group 2 was scored on NLM versus Grade Group 5 on FFPE H&E. This patient had three biopsies of the same lesion. Grade Group 5 was found on NLM in another biopsy from that lesion, which agreed with FFPE H&E.

Biopsy evaluation times decreased with increased NLM experience. Evaluation times included diagnosing, Gleason scoring, and determining the percent of biopsy involved with carcinoma. NLM evaluation times can be reduced by only evaluating biopsies for the presence or absence of carcinoma without incurring additional delays associated with Gleason scoring.

We previously reported a study using NLM to detect carcinoma in prostatectomy specimens[18]. Rapid evaluation of prostate biopsies has several challenges not present in intraoperative scenarios. First, core needle biopsies are small and fragile. Careful tissue handling and processing is required, and diagnoses must be performed using limited specimen sizes. Second, although surface artifacts can also obscure pathology in prostatectomy specimens, the small specimen sizes in biopsies makes subsurface evaluation even more critical. Finally, subtyping/Gleason scoring is less relevant for intraoperative margin evaluation but is important for diagnostics, intraprocedural feedback, and specimen triaging in biopsies.

Other groups have also demonstrated rapid evaluation of prostate biopsies using fluorescent microscopy techniques. Confocal fluorescence microscopy (CFM) has been investigated for evaluating diagnostic prostate biopsies in two separate studies of 54 and 57 patients. These studies reported an 86% sensitivity and 97% specificity[26] and a 93% sensitivity and 89% specificity[27], respectively. Other CFM studies on simulated core needle biopsies have also been reported[28]. Structured illumination microscopy was investigated on 34 core needle biopsies from radical prostatectomies that were previously frozen for tissue banking and achieved a sensitivity of 63–88% and specificity of 78–89% for detecting cancer in a two-pathologist reading[29]. Light sheet microscopy[30] and microscopy with UV surface excitation[31] have also been investigated in initial qualitative studies on simulated needle biopsies. These studies primarily restrict their analyses to the accuracy of detecting carcinoma and do not estimate accuracies of Gleason scoring. NLM uses long wavelength nonlinear fluorescence excitation and is advantageous because it enables deep, high contrast imaging in biopsy tissue[14,32]. It is important to note that none of these techniques, including NLM, are used in current clinical practice, and additional studies are needed for validation.

Limitations and conclusions

There are limitations to this study. All biopsies were performed using in-bore MRI or MRI/ultrasound fusion targeting and are therefore from a distinct group of radiologically suspicious lesions (PI-RADS scores of at least 3). There was also a limited number of patients with biopsies scored in Grade Group 5. Future studies are needed to measure accuracy of this Grade Group. Furthermore, biopsies were placed in formalin for a short period (a few minutes to 3 h) prior to NLM imaging, which would not likely be the case if performing NLM evaluation during a biopsy procedure. However, we saw no apparent differences between freshly excised tissue and biopsies that were put in formalin for a short period. The study also had a 5-month gap due to COVID-19 clinical trial stoppages. The NLM diagnostic accuracy was likely decreased after this gap due to lack of recent NLM experience. In addition, the NLM instrument used in this study is a prototype currently being developed for wider clinical use.

NLM enables accurate diagnosis and Gleason scoring of prostate core needle biopsies. NLM images closely resemble FFPE H&E and can be evaluated in real time immediately after biopsy. NLM is a promising method for real-time prostate biopsy evaluation which could provide rapid diagnostic information to patients. Future, larger-scale studies incorporating additional patients, pathologists, and institutions are needed. The technologies and methods described herein may be generally applicable to other organs and biopsy techniques.

DATA AVAILABILITY

The datasets used and/or analyzed during the current study are available from the corresponding author on reasonable request.

REFERENCES

1. Loeb, S., Carter, H. B., Berndt, S. I., Ricker, W. & Schaeffer, E. M. Complications after prostate biopsy: data from SEER-medicare. *J. Urol.* **186**, 1830–1834 (2011).

2. Essink-Bot, M. L. et al. Short-term effects of population-based screening for prostate cancer on health-related quality of life. *J. Natl. Cancer Inst.* **90**, 925–931 (1998).
3. Gustafsson, O. et al. Psychological reactions in men screened for prostate cancer. *Br. J. Urol.* **75**, 631–636 (1995).
4. Welch, H. G., Fisher, E. S., Gottlieb, D. J. & Barry, M. J. Detection of prostate cancer via biopsy in the medicare-SEER population during the PSA era. *JNCI J. Natl. Cancer Inst.* **99**, 1395–1400 (2007).
5. Masood, S. et al. Diagnostic value of imprint cytology during image-guided core biopsy in improving breast health care. *Ann. Clin. Lab. Sci.* **41**, 8–13 (2011).
6. Jacobs, T. W. et al. Accuracy of touch imprint cytology of image-directed breast core needle biopsies. *Acta Cytol.* **43**, 169–174 (1999).
7. National Cancer Institute Office of Biorepositories and Biospecimen Research. Summary: National Cancer Institute Biospecimen Best Practices Forum. Boston, MA, 2007. https://biospecimens.cancer.gov/practices/forum/boston2007/pdf/FINAL_11-05-07_NCI_BPs_Forum_Boston_Summary_Rev1-24-08_Ed.pdf.
8. Khleif, S. N., Doroshow, J. H. & Hait, W. N. AACR-FDA-NCI cancer biomarkers collaborative consensus report: advancing the use of biomarkers in cancer drug development. *Clin. Cancer Res.* **16**, 3299–3318 (2010).
9. Ahdoot, M., Lebastchi, A. H., Turkbey, B., Wood, B. & Pinto, P. A. Contemporary treatments in prostate cancer focal therapy. *Curr. Opin. Oncol.* **31**, 200–206 (2019).
10. Yang, C. & Humphrey, P. A. False-negative histopathologic diagnosis of prostatic adenocarcinoma. *Arch. Pathol. Lab. Med.* **144**, 326–334 (2020).
11. Mannweiler, S. et al. Diagnostic yield of touch imprint cytology of prostate core needle biopsies. *Pathol. Oncol. Res.* **15**, 97–101 (2009).
12. Tong, L. C. B., Rudomina, D., Rekhtman, N. & Lin, O. Impact of touch preparations on core needle biopsies. *Cancer Cytopathol.* **122**, 851–854 (2014).
13. Rekhtman, N. et al. Depletion of core needle biopsy cellularity and DNA content as a result of vigorous touch preparations. *Arch. Pathol. Lab. Med.* **139**, 907–912 (2015).
14. Denk, W., Strickler, J. & Webb, W. Two-photon laser scanning fluorescence microscopy. *Science* **248**, 73–76 (1990).
15. Yoshitake, T. et al. Direct comparison between confocal and multiphoton microscopy for rapid histopathological evaluation of unfixed human breast tissue. *J. Biomed. Opt.* **21**, 126021 (2016).
16. Cahill, L. C. et al. Rapid virtual hematoxylin and eosin histology of breast tissue specimens using a compact fluorescence nonlinear microscope. *Lab. Investig.* **98**, 150–160 (2018).
17. Cahill, L. C. et al. Comparing histologic evaluation of prostate tissue using nonlinear microscopy and paraffin H&E: a pilot study. *Mod. Pathol.* **32**, 1158–1167 (2019).
18. Cahill, L. C. et al. Nonlinear microscopy for detection of prostate cancer: analysis of sensitivity and specificity in radical prostatectomies. *Mod. Pathol.* **33**, 916–923 (2020).
19. Giacomelli, M. G. et al. Multiscale nonlinear microscopy and widefield white light imaging enables rapid histological imaging of surgical specimen margins. *Biomed. Opt. Express* **9**, 2457 (2018).
20. Giacomelli, M. G. et al. Virtual Hematoxylin and Eosin transillumination microscopy using epi-fluorescence imaging. *PLoS One* **11**, e0159337 (2016).
21. Lopez-Beltran, A., Mikuz, G., Luque, R. J., Mazzucchelli, R. & Montironi, R. Current practice of Gleason grading of prostate carcinoma. *Virchows Arch.* **448**, 111–118 (2006).
22. Reder, N. P. et al. Open-top light-sheet microscopy image atlas of prostate core needle biopsies. *Arch. Pathol. Lab. Med.* **143**, 1069–1075 (2019).
23. van Royen, M. E. et al. Three-dimensional microscopic analysis of clinical prostate specimens. *Histopathology* **69**, 985–992 (2016).
24. Verhoef, E. I. et al. Three-dimensional analysis reveals two major architectural subgroups of prostate cancer growth patterns. *Mod. Pathol.* **32**, 1032–1041 (2019).
25. Epstein, J. I., ed. *The Gleason grading system. A complete guide for pathologists and clinicians* (Wolters Kluver Health | Lipincott Williams & Wilkins, 2013).
26. Rocco B., et al. Digital biopsy with fluorescence confocal microscope for effective real-time diagnosis of prostate cancer: a prospective, comparative study. *Eur. Urol. Oncol.*, **4** 1–8 (2020).
27. Marenco J., et al. Evaluation of fluorescent confocal microscopy for intraoperative analysis of prostate biopsy cores. *Eur. Urol. Focus*, 9–14 (2020).
28. Puliatti, S. et al. Ex vivo fluorescence confocal microscopy: the first application for real-time pathological examination of prostatic tissue. *BJU Int.* **124**, 469–476 (2019).
29. Wang, M. et al. High-resolution rapid diagnostic imaging of whole prostate biopsies using video-rate fluorescence structured illumination microscopy. *Cancer Res.* **75**, 4032–4041 (2015).
30. Glaser, A. K. et al. Light-sheet microscopy for slide-free non-destructive pathology of large clinical specimens. *Nat. Biomed. Eng.* **1**, 0084 (2017).
31. Fereidouni, F. et al. Microscopy with ultraviolet surface excitation for rapid slide-free histology. *Nat. Biomed. Eng.* **1**, 957–966 (2017).
32. Helmchen, F. & Denk, W. Deep tissue two-photon microscopy. *Nature* **2**, 932–940 (2005).

ACKNOWLEDGEMENTS

We thank Daniela Tridente, Pei-Kang Wei, Michael Johnson, Maureen Frederick, and Alexander Goehler from the Department of Radiology, BIDMC for their help collecting biopsy specimens. This study was supported in part by the National Institutes of Health R01-CA178636-06, R01-CA249151-01, and the MIT Termeer Medical Engineering Graduate Fellowship.

AUTHOR CONTRIBUTIONS

L.C.C., S.R., T.Y., Y.W., L.L.T, B.G., J.G.F., Y.S. performed study concept and design, development of methodology and writing, review and revision of the paper; All authors acquired, analyzed and interpreted data; All authors read and approved the final paper.

COMPETING INTERESTS

J.G.F., T.Y., and L.C.C. are inventors on US patent no. 10416434: Method and apparatus for imaging unsectioned tissue specimens. The remaining authors declare no competing interests.

ETHICS APPROVAL AND CONSENT TO PARTICIPATE

Written informed consent was obtained from all subjects. All research was performed according to protocols approved by Beth Israel Deaconess Medical Center Committee on Clinical Investigations and Massachusetts Institute of Technology Committee on the Use of Humans as Experimental Subjects.

ADDITIONAL INFORMATION

Supplementary information The online version contains supplementary material available at https://doi.org/10.1038/s41379-021-00960-1.

Correspondence and requests for materials should be addressed to Yue Sun.

Reprints and permission information is available at http://www.nature.com/reprints

Publisher's note Springer Nature remains neutral with regard to jurisdictional claims in published maps and institutional affiliations.